Contents list available at Journal of e-Science Letters

Journal of e-Science Letters

journal homepage: http://scienceletters.researchfloor.org/

Activation Process and Sorption Properties Analysis of NEG Materials

K. Surendra*, G.V.V. Satyanarayana, A.D.P. Rao

Department of Nuclear Physics, Andhra University, Visakhapatnam- 530003, India

ARTICLE INFO

Article History:
Received 20 June 2022
Revised 18 August 2022
Accepted 02 September 2022
Available Online 05 September 2022

Keywords:
Vacuum,
Ti-Co, and Zr-Co NEG materials,
absorption,
desorption,
thermal analysis.

ABSTRACT

This article briefly describes the preparation of Ti-Co and Zr-Co NEG alloys with the chemical composition Ti700+x+Co297-x+(Sm+Gd)3 and Zr700+x+Co297-x+(Sm+Gd)3, where X=0, 40, 80, 120 in steps. These are made using a traditional solid-state reaction method and activated at a temperature of 1000°C. These are analyzed with X-ray Diffraction (XRD) for structural analysis, Field Emission Scanning Electron Microscope (FESEM) with Energy Dispersive Spectroscopy (EDS) for morphological and elemental concentration analysis, Transmission Electron Microscopy (TEM) for micro-structural and average particle size analysis, Thermogravimetric Analysis (TG/DTG), and Differential Scanning Calorimeter (DSC) for gas absorption or desorption characteristics studies. The main objective of this research is to investigate the activation process and the gas absorption or desorption (sorption) investigations of the Samarium (Sm) and Gadolinium (Gd) substituting rare-earth components in Ti-Co and Zr-Co NEG alloys.

1. Introduction

In the past few years, many NEG alloys have been used for different applications in vacuum technology [Xu, Yaohua et al (2016); Xiong, Y. H.,et al (2008); Xu, Yaohua et al (2016)]. For these reasons, the Zr-V-Ti, Zr-V-Fe, Zr-Al, and Zr-Co non-evaporable getter alloys were widely used to achieve better vacuum-type devices [Xu, Yaohua et al (2006); ZHOU, Hong-guo, et al (2007); Petti, Daniela, et al (2010]. Also, these are supports inside chemical reactions of getter and gases to maintain good vacuum conditions in the machines [Zhou, Chao, et al (2020); Petti, Daniela, et al (2010)]. The primary need for non-evaporable getter materials is low activation temperature, high resolvability limitation and high conductivity to the absorbed categories, high temperature, and high chemical strength. The NEG materials with the lowest activation temperature are Ti-Co and Zr-Co alloys [Zhang, Y.,et al (2009); Deng, Guangxia et al (2013); Moghadam, A. et al (2015)]. Therefore, NEG materials are essential for obtaining and maintaining vacuum conditions for ultra-high or extremely ultra-high vacuum (UHV) systems. This paper discussed the structure, morphologies, microstructure, and gas absorption or desorption performance of substituting rare-earth components Sm and Gd of NEG getter materials [Yoozbashizadeh,et al (2015); Bu, J. G., et al (2012) Bandyopadhyay, et al (2000)].

*Corresponding Author: K. Surendra
E-mailAddress:keth.surendra@gmail.com
http://dx.doi.org/10.46890/SL.2022.v03i04.002

2. Experimental Details of NEG Materials

The composition of the NEG getter alloys is derived from stoichiometry ratios starting with Ti, Zr, and Co metal powders from Sigma Aldrich (99.99%) and rare-earth (RE) components Samarium and Gadolinium metal powders from Merck (99.99%). The chemical compositions are $Ti_{700+x}+Co_{297-x}+(Sm+Gd)_3$ and $Zr_{700+x}+Co_{297-x}+(Sm+Gd)_3$ synthesized, where X=0, 40, 80, 120 in steps. The mixed raw powder material was first thoroughly grinded for 15 hours using an

agate mortar and pestle to add methanol solvent for bind the substance. This combined powder material was heated in a muffle box furnace for 1 hour at 350°C to remove the moisture content in the metal powder. When the heated powder material has cooled to come room temperature, it is grinding again for 1 hour to make the materials well blended. These materials were then formed into pellets in circular discs using a KBr Hydraulic Pellet Presser with a pressure of 3 tons for 5 minutes on the pellet machine to generate NEG alloys. These are sintered in a muffle furnace at 1000°C for 2 hours to make non-evaporable getter alloys. The XRD patterns of both series of materials were obtained using a Panalytical X-pert pro-diffract-meter with diffraction angle 2θ ranging from 10° to 80° in 0.02° steps. The alloy's spectra were acquired using thermogravimetric analysis (TGA) and differential scanning calorimeter (DSC) techniques. By studying the weight growth, endothermic and exothermic peak behaviors of the NEG materials, these measurements can better understand the gas absorption capabilities. The current measurements were carried out with the Mettler Toledo TG/DTG 851e apparatus, which has a temperature range of ambient temperature to 1000°C in a nitrogen gas atmosphere with a heating rate of 10°C/min at a constantly applied pressure. A transmission electron microscope (TEM) made by the Philips Company, a scanning electron microscope (SEM), and an energy dispersive spectrometer (EDS) made by JEOL were used to look at the materials' shapes and how they were made.

3. Results and Discussion

3.1 X-ray Diffraction Studies

The XRD technique is a universally accepted method to determine the behavior of the crystal and its structure. The material is basically in the form of powder, comprising fine particles of material with a single crystalline to be studied. This technique is extensively utilized for structure analysis, structure determination, crystallite size, lattice constant, texture and electron radial distribution functions. The XRD analysis for the synthesized getter material is carried out to study the relation between crystallographic properties and their variation with rare earth elements substitution. The lattice constant and XRD patterns measure the cell volume of each

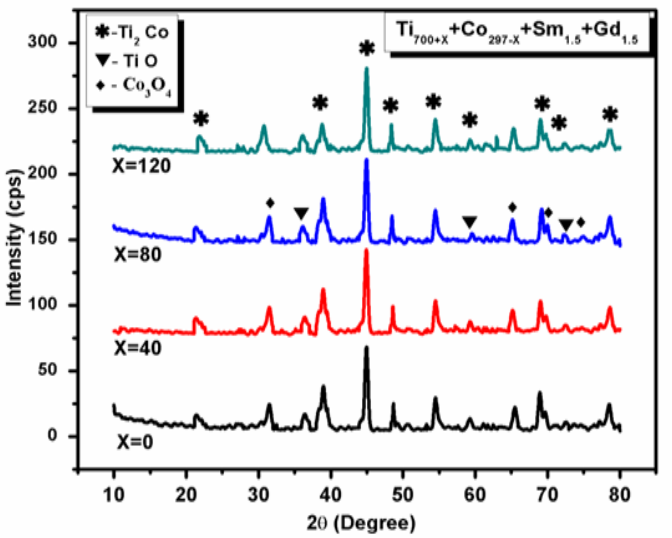

Fig.1: XRD patterns of (Ti-Co-RE) series alloys. .

sample to assess the influence of RE element replacements on the crystalline lattice of the fine getter materials developed.

The obtained X-ray diffraction patterns for the (Ti-Co-RE) and (Zr-Co-RE) series of NEG materials are depicted in Fig.1 and 2 respectively. The (Ti-Co-RE) series observed to contain 9 major fingerprint peaks found around 2θ = 22.72°, 38.97°, 44.19°, 47.58°, 54.49°, 59.87°, 69.14°, 73.16°, and 79.51° with the h,k,l values are (1 1 1), (2 2 0), (3 1 1), (2 2 2), (4 0 0), (3 3 1), (4 2 2), (5 1 1) and (4 4 0) legibly identified with JCPDS Card No # 00-152-5181. It is interesting to note the four strong peaks found around 2θ = 38.97°, 44.19°, 54.49° and 69.14° are corroborated with the earlier investigations. With the decrease of Co content in the chemical composition, the major diffraction peaks are shifted to the lower angle side. Unit Cell software calculates the values of their related Bragg angles and the lattice parameter. The crystallite sizes of the (Ti-Co-RE) getter materials are determined using the Debye-Scherrer formula based on the FWHM of the most intense diffraction peak (3 1 1) [Rostoker, W., et al (1952); Yu, T.-H. Lin, S.-J. et al (1972); Phromma, Siripond, et al (2020)]. All of these values are listed in the Table.1.

The present materials have been determined to have cubic phases (Ti_2O) of the face-centered cubic (FCC) type, which have the same structure as ß-titanium with the space group Fd-3m. With a drop in Co concentration, the lattice constant, lattice volume, and crystallite sizes rise, whereas concentration increases [Rostoker, W., et al (1952)]. The obtained average values of crystallite size are in the range of 11.00 nm to 13.00 nm, as shown in Table1. The increase of crystallite size,

Table1: Lattice parameter, Unit cell volume, Crystallite size values and Intensity of synthesized

$Ti_{640+x}+Co_{297-x}+(Sm+Gd)_3$ where x varies between x=0 to 120 insteps of 40							
value (X)	M ax Peak h k l (31 1) 2θ (deg)	d(Spac-ing)Å	Lattice Constant "a" (Å)	FWHM θ (deg)	Volume (V cm^3)	Crystallite Size (nm)	Intensity (I)
0	44.72	2.02	6.69	0.75	300.76	11.41	96
40	44.78	2.04	6.76	0.74	309.72	11.50	94
80	44.86	2.05	6.78	0.73	312.01	11.74	109
120	44.95	2.06	6.83	0.71	318.92	12.17	118

(Ti-Co-RE) NEG materials.

Table2: Lattice parameter (a), Unit cell volume, Crystallite size values and Intensity of synthesized (Zr-Co-RE) NEG material.

$Zr_{640+x}+Co_{360-x}+(Sm+Gd)_3$ where x varies between x=0 to 120 insteps of 40							
value (X)	MaxPeak h k l (1 1 2) 2θ (deg)	d(Spacing)Å	Lattice Constant "a" (Å)	FWHM θ (deg)	Volume (V cm^3)	Crystallite Size (nm)	Intensity (I)
0	34.18	2.56	**a**=3.44	0.59	328.92	14.09	170
40	34.74	2.57	**b**=10.86	0.57		14.40	180
80	34.86	2.59		0.56		14.67	197
120	34.95	2.62	**c**=8.98	0.54		15.31	254

particularly for lower concentrations of cobalt, increases the surface area of the materials. Contrary to this, lattice parameter (a) and unit cell volume were found to increase with the decreased content of cobalt. Significantly starting composition of the alloy with lower Ti and higher Co contents too found to show higher values of all the parameters such as crystallite size, lattice parameter (a), and unit cell volume [Phromma, Siripond, et al (2020)]. These may be understood based on the crystalline nature of cobalt and titanium elements.

In the XRD pattern, small diffraction peaks of (TiO) phase exhibiting cubic structure and 2θ=36.46°, 59.63°, and 72.58° corresponding to h,k,l values are (1 1 1), (2 2 0), and (3 1 1) were observed with JCPDS card no.00-153-6851. Other small diffraction peaks of the Co_3O_4 cubic phase observed at 2θ=31.18°, 65.78°, 70.19°, & 74.66° corresponding to the h,k,l values are (2 2 0), (4 4 0), (6 0 0), and (6 2 0) planes, respectively (JCPDS card no.00-152-6734). When Ti concentration was increased to 120%, the intermetallic decreased. The RE effect should be observed clearly in the lattice parameter, unit cell volume and crystalline size, which are increasing [Wu, Jun. "In-situ, et al (2012); Sato, Shintaro, (2005); Straumal, B. B., A. et al (2018); Behnajady, Mohammad A et al (2015)]. The prepared (Ti-Co-RE) by traditional heating has the standard value of lattice parameter 6.7300 Å. It is clear that our calculated experimental lattice parameter increases with the addition of rare elements. The NEG materials should benefit from this. The small amount of amorphous crystallite regions in Fig. 1 decreases the FWHM of the diffraction peaks according to Scherrer's formula [Bamne, Jyoti, et al (2018); Song, Ho-Jun, et al (2014)].

Fig.2 shows the XRD pattern of (Zr-Co-RE) getters at different concentrations prepared at a sintering temperature of 1000°C. This series observed to contain 11 major fingerprint peaks at 2θ=20.15°, 27.40°, 32.93°, 34.17°, 38.47°, 43.71°, 47.79°, 53.97°, 63.07°, 69.20°, and 75.93° the observed h,k,l values

are (0 0 2), (1 1 0), (0 4 0), (1 1 2), (1 3 1), (0 2 4), (1 3 3), (0 2 5), (2 2 2), (0 8 0) and (1 7 3) these legibly identified with JCPDS Card No # 00-152-4752. It is interesting to note the five strong peaks found around 2θ = 34.17°, 38.47°, 43.71°, 53.97° and 75.94° are corroborated with the earlier investigations [26-28]. The orthorhombic structure Zr_3Co, which has a stronger activation condition, is a base-centered orthorhombic system that permits translation in one of the base planes and the related space group Cm cm (63). The values of their corresponding Bragg angles and the lattice parameter (a) can be calculated by using Unit Cell software. By using Debye-Scherrer's the crystallite sizes of the present (Zr-Co-RE) alloys are evaluated based on the FWHM of the most intense diffraction peak (1 1 2) equation [Xu, Yaohua , et al (2016); Petti, Daniela, et al (2010); Yoozbashizadeh, et al (2015); Bu, J. G., et al (2012)]. All these values are listed in Table 2. At higher sintering temperatures, the crystalline size increases with increasing Zr concentration. The d-spacing and intensities increase when the Zr concentration is increased. The FWHM is decreased when the Co concentration is decreased [Kripyakevich, et al (1970); Suyama, et al (1987); Lambert, et al (2001)].

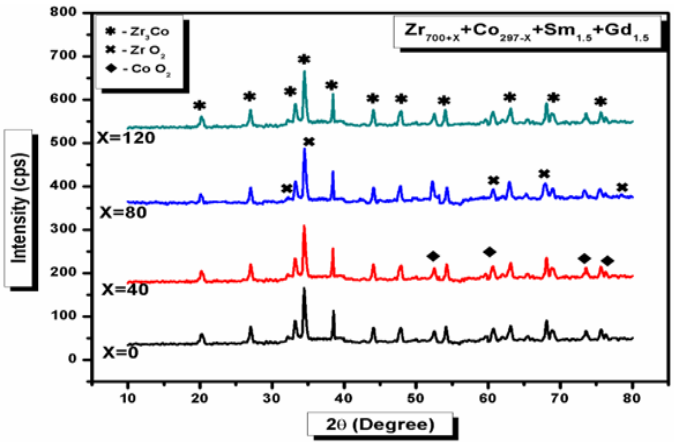

Fig.2: XRD patterns of (Zr-Co-RE) series alloys.

The average crystalline size of the getter alloys was estimated to be 14.05 nm to 15.05 nm, respectively. The standard average lattice parameters of the orthorhombic crystal structure are a=3.27Å, b=10.84Å and c=8.95Å. Also, the volume is 317.25Å^3. This significantly enhances the absorption capacity of these alloys. Other small diffraction peaks of ZrO_2 phases are the orthorhombic structure which can be observed at 2θ=33.84°, 35.12°, 61.29°, 68.38° and 78.94° corresponding to h,k,l values (0 2 0), (0 0 2), (3 1 1), (1 2 3) and (3 3 0) planes respectively (JCPDS card no. 00-154-5065). Another small diffraction peak of the CoO_2 phase, which is orthorhombic structure, was observed at 2θ=52.85°, 61.05°, 75.42°, and 77.19°corresponding to h,k,l values (2 0 9), (2 0 11), (0 2 8) and (2 0 15) planes respectively (JCPDS card no. 00-152-6822). This could significantly enhance the sorption capacity of these alloys [Zhao, Zhenmei, et al (2009); Petti, Daniela, et al (2010); Heshmatpour, et al (2011); Qian, Z., et al (1998)].

3.2 Thermal Analysis (TG/DTA and DSC)

Thermogravimetric analysis (TG/DTA) measures the mass changes in a compound as temperature varies and is mainly used to determine phase transitions in materials. The TG graphs are often plotted as temperature against mass change percentage. A differential weight growth curve (DTA) helps to determine the phase transition temperature by recognizing the point where weight gain is most visible. These tests were carried out in nitrogen gas, with the powder materials being heated to a maximum temperature of 1000°C at a rate of 10°C/min. The DSC determines how much energy (heat) the sample absorbs or releases when heated, cooled, or stored at a moderate temperature. The melting point, crystallization, glass transition, and oxidation time are all measured using DSC. It is a standardized DSC test that determines the level of stabilization of material assessments [Song, Ho-Jun, et al (2014)]. Finally, thermal investigations demonstrate how the material's properties are affected by temperature. This section focuses on thermally induced modifications, occurrences, transformations, and reactions to better understand the synthesis mechanism.

The TG/DTG and DSC graphs for the synthesized compositions of $Ti_{700+x}+Co_{270-x}+(Sm+Gd)_3$ and $Zr_{700+x}+Co_{270-x}+(Sm+Gd)_3$ (where x varies in steps of 040 between x = 0, 40, 80, 120) non-evaporable getter materials are shown in the Fig. 3 & 4. These four types of samples of pure 99.9% (Ti-Co-RE) substance with different weights (a) 4.3mg at X=0 (b) 4.2mg at X=40 (c) 4.1mg at X=80 (d) 4.4mg at X=120 and (Zr-Co-RE) substance with different weight (a) 4.5mg at X=0 (b) 5.1mg at X=40 (c) 4.6mg at X=80 (d) 4.9mg at X=120, were used for TG/DTA analysis. Also, the four types of samples

pure 99.9% (Ti-Co-RE) substance with different weights (a) 5.1mg at X=0 (b) 4.6mg at X=80 (c) 5.4mg at X=80 (d) 4.7mg at X=120and (Zr-Co-RE) substance with different weight (a) 4.8mg at X=0 (b) 5.3mg at X=40 (c) 4.4mg at X=80 (d) 5.2mg at X=120, were used for DSC analysis.

In the series of (Ti-Co-RE) getter materials, the nitrogen-sorption characterization was investigated by heating the getter sample from the temperature 30˚C to 1000˚Cwith flowing nitrogen atmosphere with a heating rate of 10˚C/min by thermogravimetric analysis. In this, it is observed that in the first step of TG curves in Fig.3, a small weight decreases with increasing temperature from 30˚C to 200˚C; this indicates that desorption of physisorbed gas molecules (the physical bonding of gas molecules to the surface of the getter alloy) [Li, Chien-Cheng, et al (2006)]. The next small slope from the temperature range of 200˚C to 280˚C is due to an increase in sorption. The third slope located from the temperature 280˚Cto 450˚C is due to equilibrium of weight established due to nitrogen sorption and desorption of chemisorbed water vapor. The fourth bigger slope is located from 450˚C to 950˚C is due to continuous nitrogen sorption to the getter alloy [Wesley W.M. (1986)]. All the slopes in Fig.3, getter materials are almost the same; the increase in the weight is due to the adsorption of nitrogen molecules on the surface of the getter material samples. The larger weight gain of the (Ti-Co-RE) getter material is due to its higher absorption capacity observed for an increase in titanium metal powder weight and decrease in the cobalt metal powder weight and higher surface area of this kind of getter material [Surendra, K., et al (2021)]. The reaction mechanism of the nitrogen absorption on (Ti-Co-RE) getter materials contain many compound reactions, such as absorption and desorption on the sample's surface reaction rate between nitrogen and surface of the metal powder and distribution rate of nitrogen atoms in the getter material. After a higher sample temperature from 450˚C to 950˚C with flowing nitrogen increases the weight of the getter materials (Ti-Co-RE). The total weight gain in all TG curves estimated to be (a) 0.102 mg at X=0, (b) 0.104 mg at X=40, (c) 0.106 mg at X=80, and (d) 0.113 mg at X=120 concentrations. The alloy takes on an extreme solid form after being heated to a higher temperature of 1000˚C also it is thermally stable [David R. Gaskell, (1995)].

The differential thermal analysis (DTA) curve is displayed against temperature and DTA-uV. The DTA curves of these non-evaporable getter materials exhibit two kinds of phase shifts due to their composition (Ti-Co-RE) when the temperature increases from 30˚C to 540˚C. On the positive axis side and from 540˚C to 980˚C. On the negative axis side, two-phase peaks are created that are the spinel phases for the non-innovate

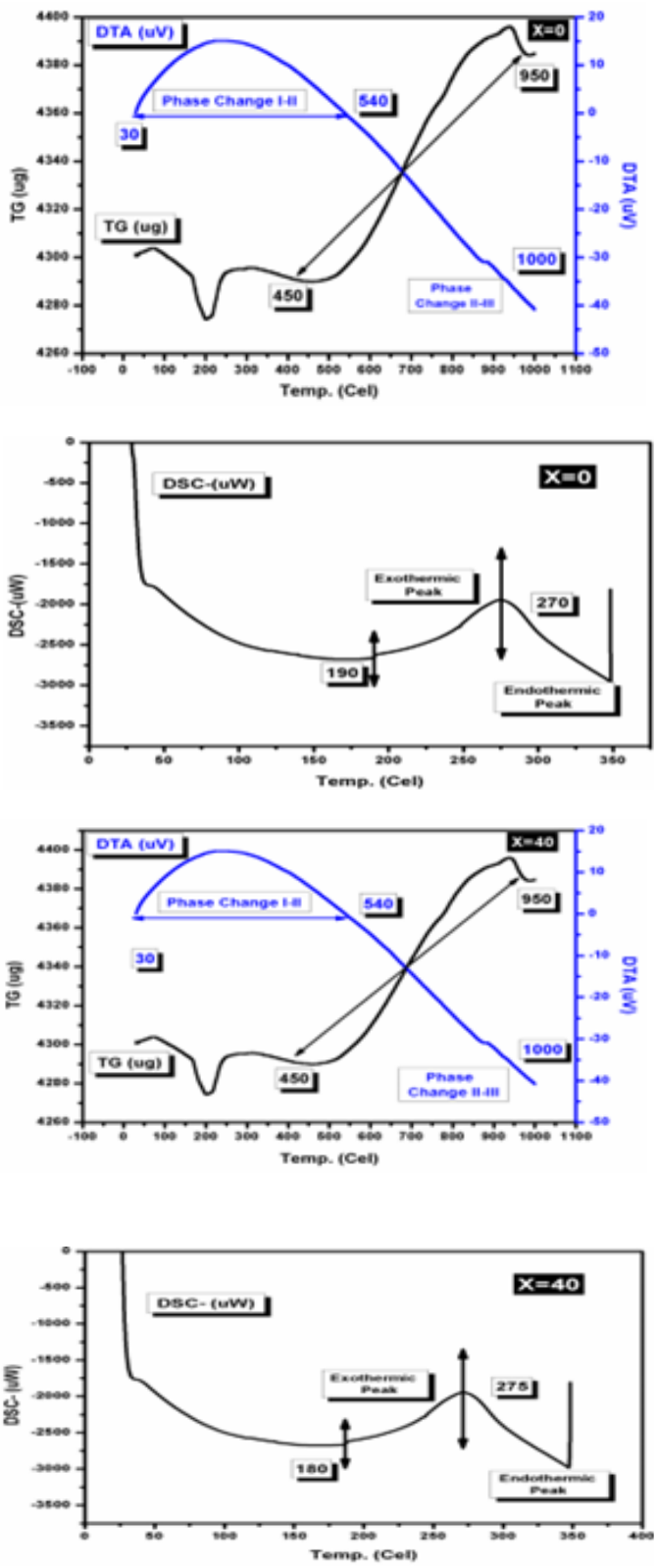

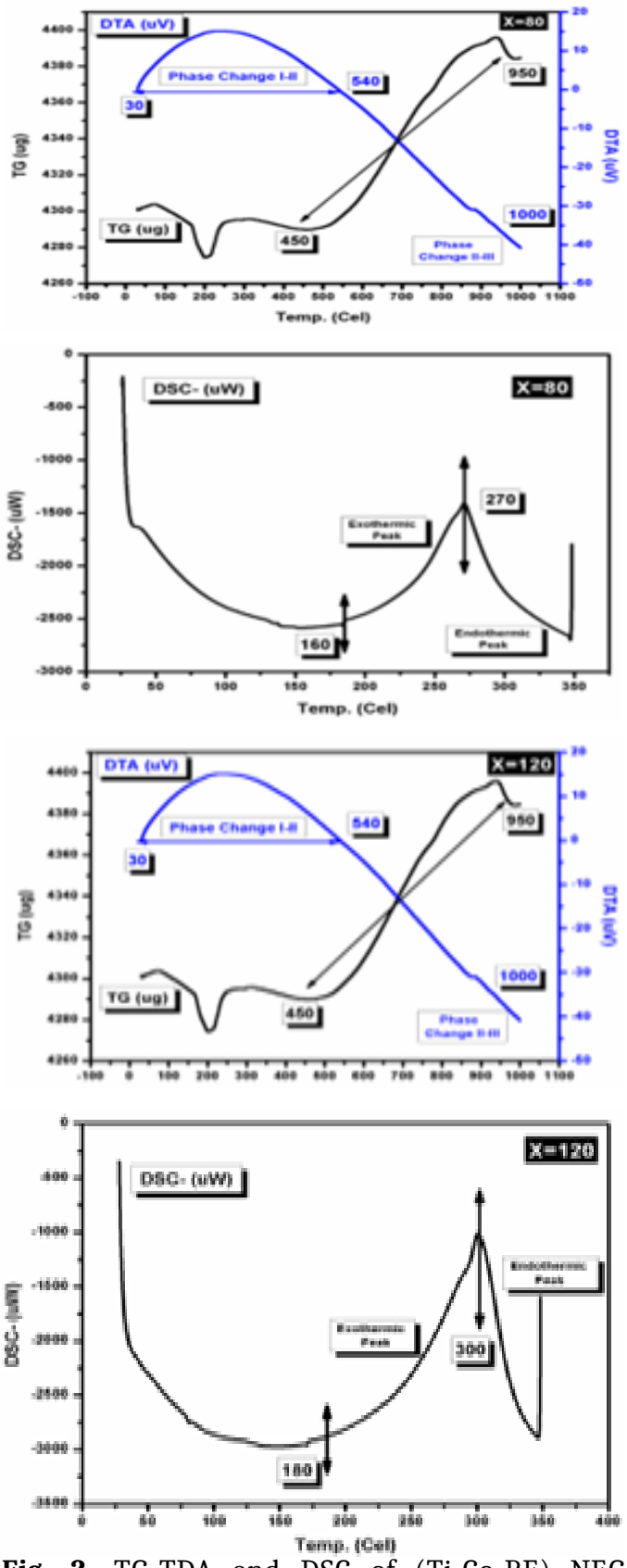

Fig. 3. TG-TDA and DSC of (Ti-Co-RE) NEG material results.

of these NEG compounds [Li, Chien-Cheng, et al (2006)]. Due to the exothermic or endothermic changes in the solid-state processes, the phase I-II positive side and phase II-III negative side can alter between these temperatures. The DTA investigations demonstrate that the exothermic reaction between the metal alloy and nitrogen occurs between 250˚C and room temperature due to the absorption in Phase I-II. The endothermic reaction occurs when the temperature is between 540˚C and 1000˚C in phases II-III.

In Fig. 3, the corresponding differential scanning calorimetry (DSC) curves of the (Ti-Co-RE) composition are presented. There are notable exothermal curve plots between 180˚C and 300˚C, which are connected to the reaction of the getter alloy with nitrogen gas molecules. However, there is a broad endothermic peak for the getter materials between 300˚C and 350˚C. The reaction between nitrogen gas and NEG alloy causes the exothermal peak. The (Ti-Co-RE) getters' reducing reaction is related to the endothermic peak. According to the findings, activation at 350˚C for an hour reduced oxidized (sorption) of (Ti-Co-RE) on the alloy's surface to a metallic state. The oxidized titanium still communicates extremely well, though.

The results from the oxidized titanium displacement reaction and Fig.3 show the exact results. The weight gain studies in the following nitrogen gas by the thermogravimetric measurement demonstrate the mechanism of nitrogen absorption or adsorption and surface reaction. The non-evaporable getter base material has a higher capacity to absorb the residual gases of oxygen, nitrogen, carbon, hydrogen etc. [J.T. Ellingham, (1994)]. The nitrogen-sorption characterization of the second series of (Zr-Co-RE) getter materials was investigated by heating the getter sample from room temperature 30˚C to 1000˚C in flowing nitrogen atmosphere with a heating rate of 10°C/min by thermo-gravimetric analysis. It is observed that in one-step of pure (Zr-Co-RE) samples of TG curves in Fig.4, there is a flat top (thermally equilibrium stage) from the temperature from 30˚C to 310˚C; this is the desorption of physisorbed gases (the physical bonding of molecules to the surface of the getter alloy). The next second highest slope located from the temperature range of 310˚C to 950˚C indicates sorption of nitrogen continuously increases to the getter alloy; this can be observed in Fig. 4 of TG curves [Larson, Erica J., et al (2002)]. The increased weight the getter materials (Zr-Co-RE) in all TG curves shows a total weight gain of approximately estimated that of (a) 0.622mg at X=0, (b) 0.475mg at X=40, (c) 0.672mg at X=80, and (d) 0.263mg at X=120 concentrations respectively. After heating at a higher temperature of 1000°C for TGA

analysis, the alloy shows a powerful solid form. It shows thermally most stable. The DTA is the same as the previous series (Ti-Co-RE) for the phase changes [Keiteb, Aysar S., et al (2016); Naseri, Mahmoud Goodarz, et al (2011)].

Fig. 4 shows the corresponding differential scanning calorimetry (DSC) curves for the composition of (Zr-Co-RE). When the getter alloy

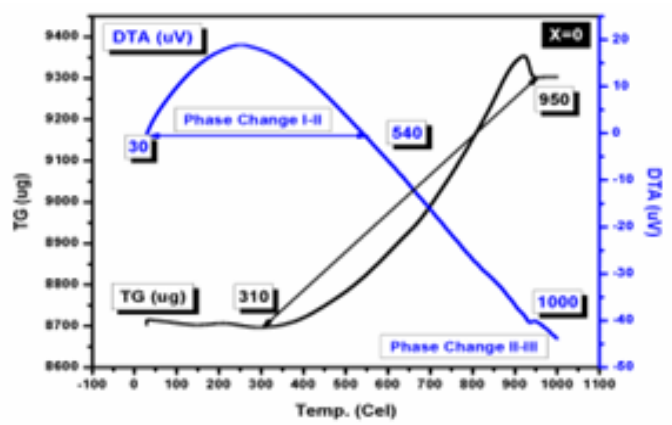

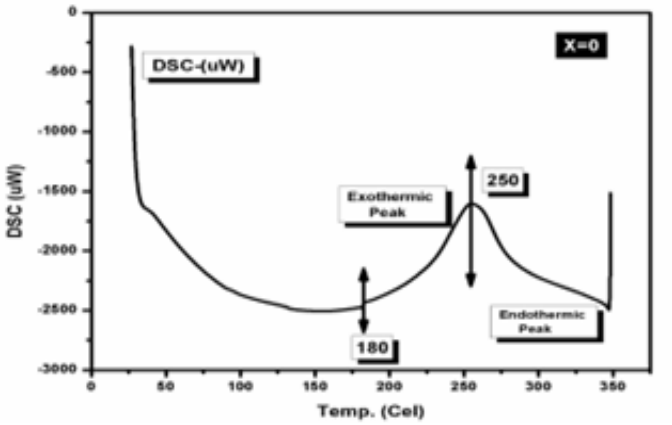

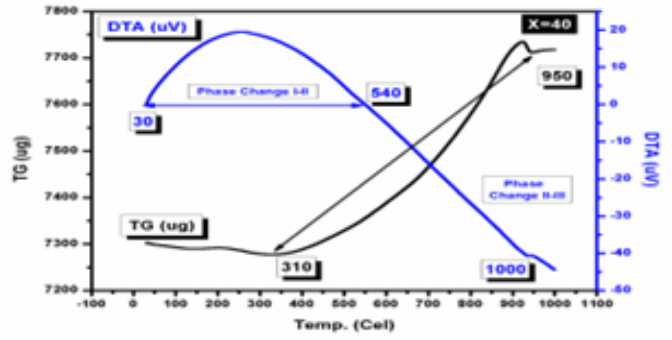

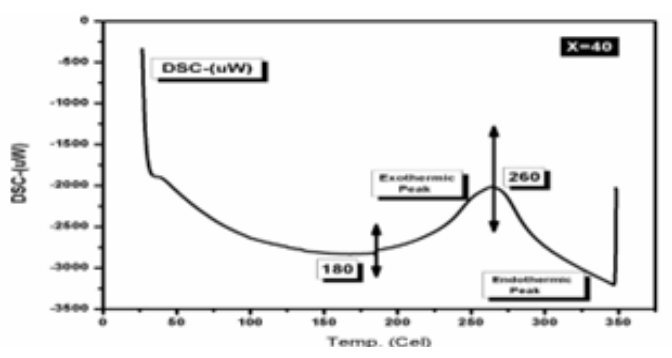

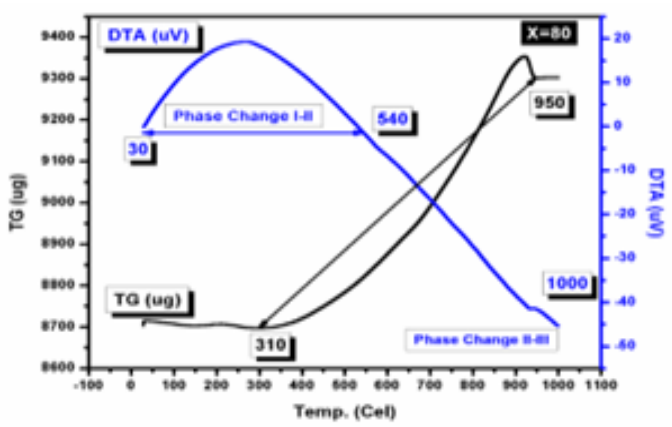

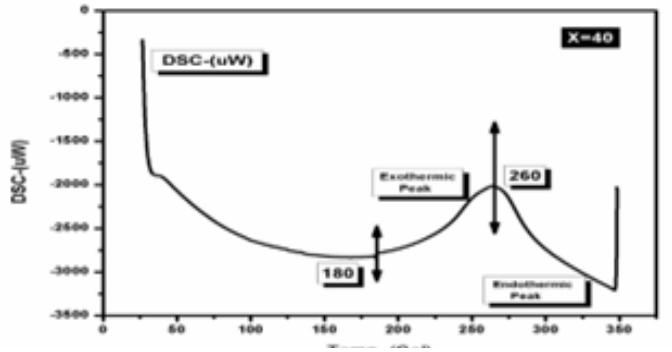

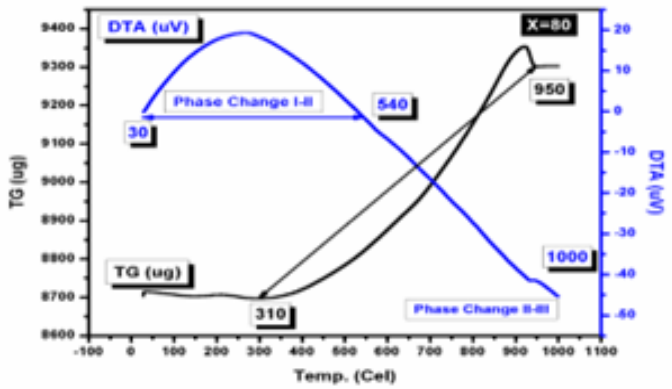

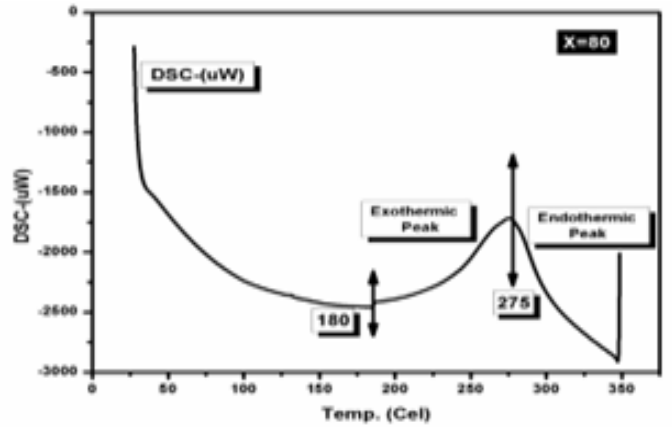

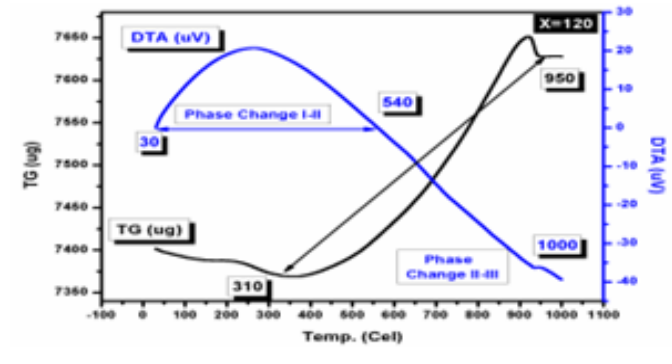

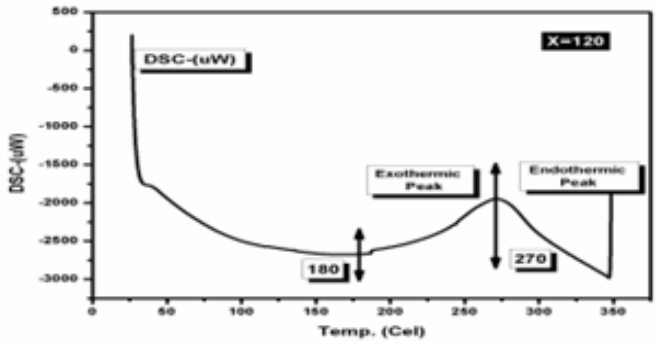

Fig. 4. TG-TDA and DSC of (Zr-Co-RE) NEG material results.

reacts with nitrogen gas molecules, there are notable exothermal peaks for the curves between 180˚C and 250˚C and 275˚C for all plots. In contrast, a broad endothermic peak in the temperature range of 275˚C to 350˚C is shown for the getter materials. The reaction between the NEG alloy and nitrogen gas produced the exothermal peak. The reducing reaction of the (Zr-Co-RE) getters is related to the endothermic peak. [GoodarzNaseri, et al (2010); Garcia, JoelsonCott, L. et al (2006); Yun, S. H., S. Cho, M. H. (2010); S. Konish et al, (1995)]. According to the findings, activation at 350˚C for an hour reduced the oxidized (sorption) surface of (Zr-Co-RE) alloys to an elemental phase. But the oxidized zirconium still communicates quite effectively. The oxidized titanium's displacement reaction causes this, and the complete findings are shown in Fig. 4. Thermogravimetric examination of weight increase tests in flowing nitrogen reveals the mechanisms of nitrogen absorption or adsorption and surface response, respectively. The ability of the non-evaporable getter metal powder to absorb leftover oxygen, nitrogen, carbon, and hydrogen gases is increased [N. Bekris et al, (2006); Yuan, Peng, et al (2019); Valdre, G., D. et al (1999)].

3.3 SEM with EDS (EDX) Analysis

The typical SEM images of RE substituted spinel structured Ti_{700+x}+Co_{297-x}+$(Sm+Gd)_3$ and Zr_{700+x}+Co_{297-x}+$(Sm+Gd)_3$ is shown in Fig.5 & 6. The SEM uses a scanning electron beam to characterize the morphology of the synthesized samples. In this technique, a beam of electrons from an electron gun interacts with the sample. Energy is exchanged between the electron and the material, producing high-energy electrons and extra electrons due to elastic and inelastic scattering. Thus, the SEM produces structural images of the samples and the size in the range of micro-meters [Xu, Yao Hua, et al (2019); Ashiri, R. (2013)]. The surface elemental analysis is carried out using (EDX) apparatus attached to the SEM. With the high activation temperature of 1000˚C for 60 minutes, the (Ti-Co-RE) & (Zr-Co-RE) getter powders, the nucleated crystalline has seen the surface of the synthesized getter powder grow, and particle size distribution becomes narrower [Ashiri, Rouholah. (2012); Zavaliy, I. Yu, R. et al (2005)]. SEM images show the formation of nano-crystalline cubic (Ti_2Co phase) and orthorhombic (Zr_3Co phase) structures [Heyder, R., L., et al (1996)]. In both series, the grain size seems to have grown to be in the 10 nm to 15 nm range.

Additionally, it is discovered that the size grows in the NEG samples as replaced RE increases, which is strongly associated with the XRD pattern. The homogenous particle size distribution of the NEG materials suggests that they have good crystalline nature and are in good agreement with the XRD pattern. Every SEM image reveals that the resulting surfaces are porous, with particles with metallurgical structure. These getters increase the specific surface area, gas sorption capacity and gives minimal strength requirements. In addition, every sample that has been prepared has a porous structure that allows gas atoms to diffuse through getter materials more efficiently.

The structural stability of the (Ti-Co-RE) and (Zr-Co-RE) non-evaporable getter materials are investigated using EDS. Besides the free energy deposition of Ti, Zr, Co, and RE oxides, no other impurity peaks were exhibited in the spectra, as shown in Fig.7 and 8, showing that the most stable compounds are more than TiO_2, ZrO_2, and Co_2O_2. The dissociation of Ti, Zr oxides and RE oxides occur when the NEG getter materials are heated to a high temperature of 1000˚C, which is beneficial for getter activation. The tables indicate the proper atomic and weight percentage ratios measured by both series.

3.4 Morphology and Size Distribution by using (TEM)

Microstructure and related parameters such as average grain size and grain growth type, which determine the mechanical strength of materials, can be aided by morphological analysis. For RE substitution (Sm & Gd), the obtained micrographs of the (Ti-Co-RE) and (Zr-Co-RE) series of non-

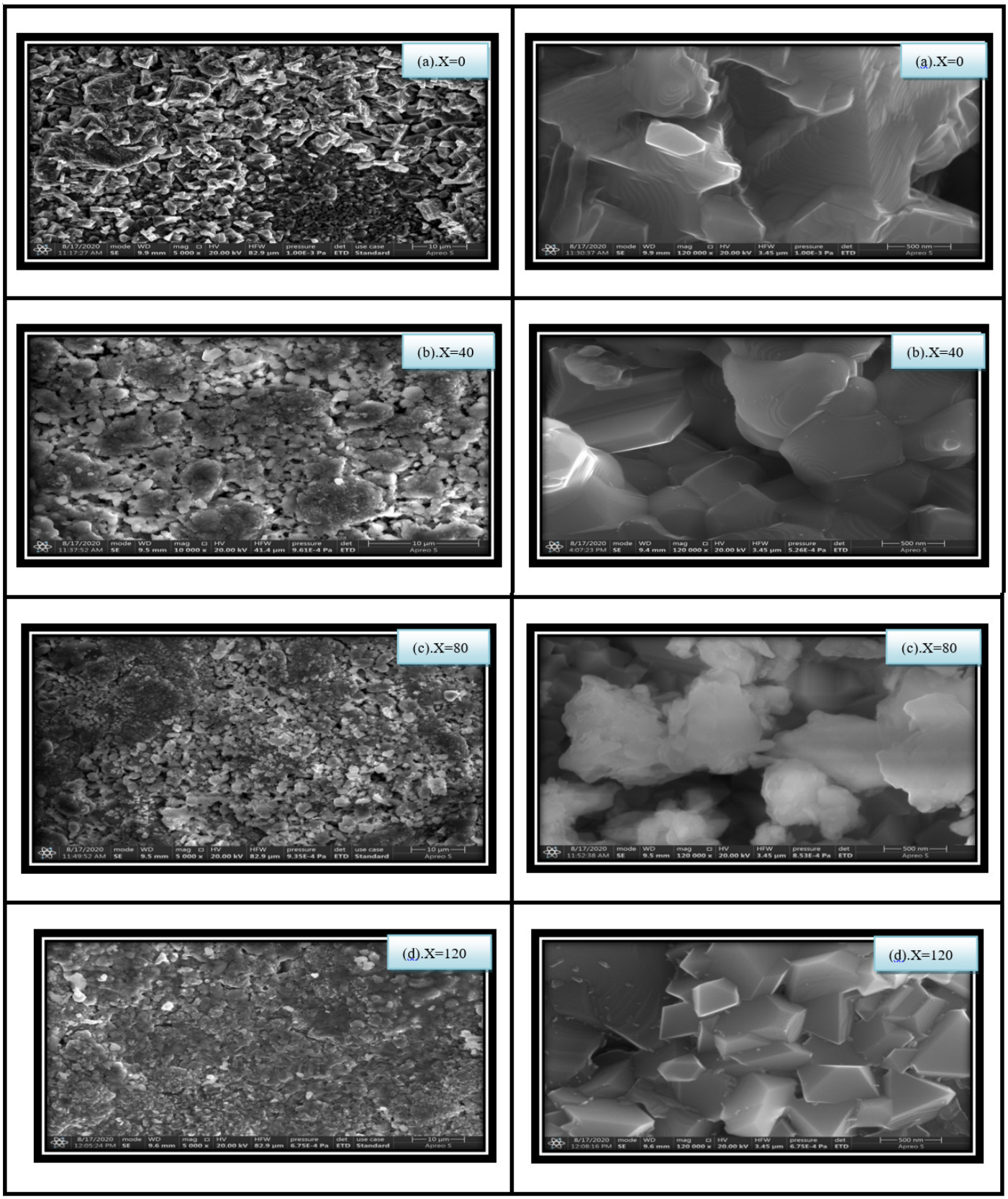

Fig. 5. Results of SEM micrograph of (Ti-Co-RE) NEG material.

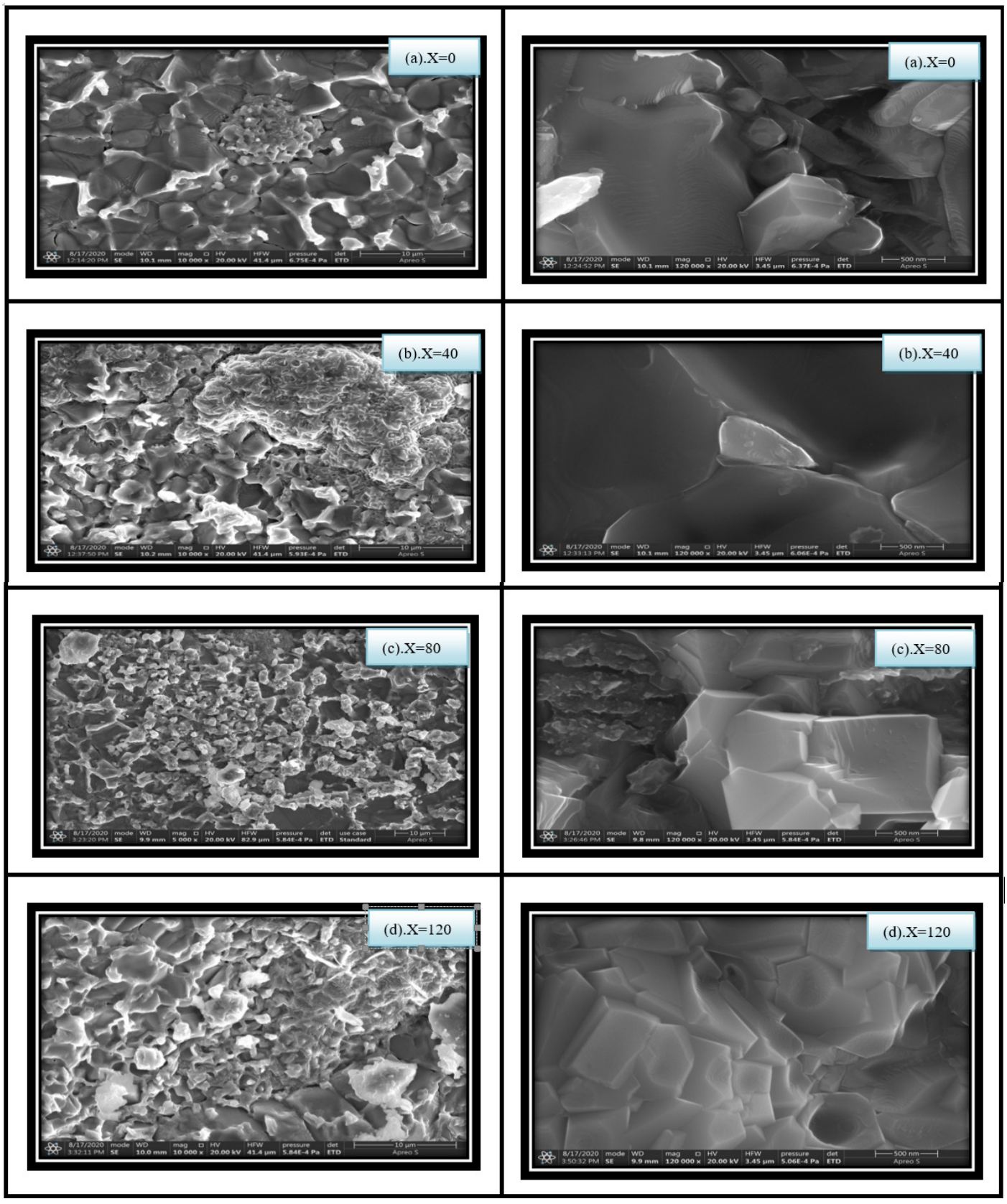

Fig. 6. Results of SEM micrograph of (Zr-Co-RE) NEG material.

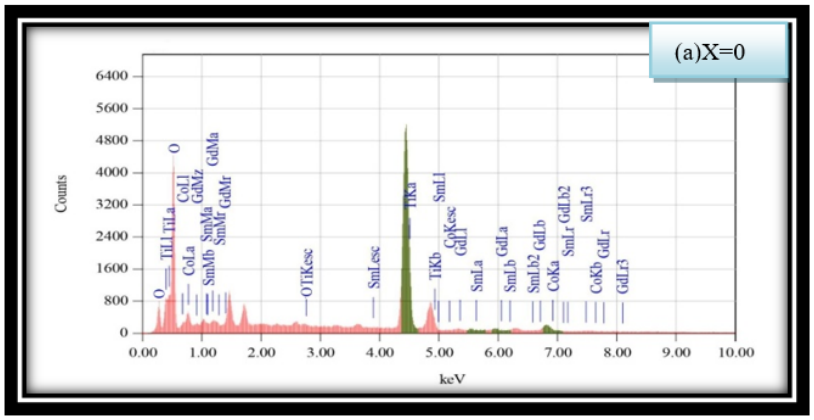

Element line	Weight %	Atom %
Ti K	85.74	87.91
Co K	12.45	10.11
Sm K	0.96	1.02
Gd K	0.85	0.98
Total	100.00	100.00

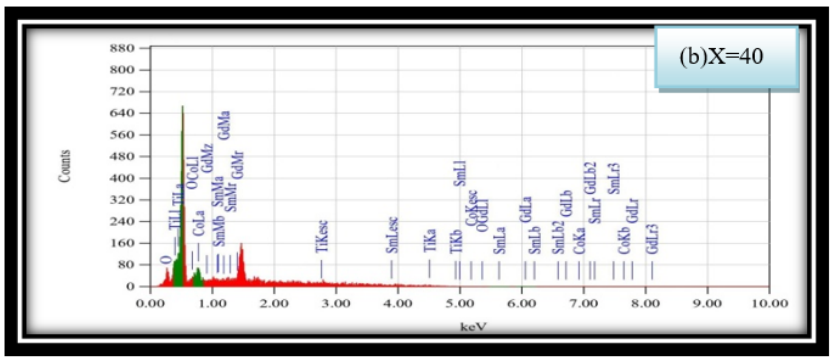

Element line	Weight %	Atom %
Ti L	79.91	85.86
Co L	19.08	12.48
Sm L	1.13	0.84
Gd L	1.01	0.82
Total	100.00	100.00

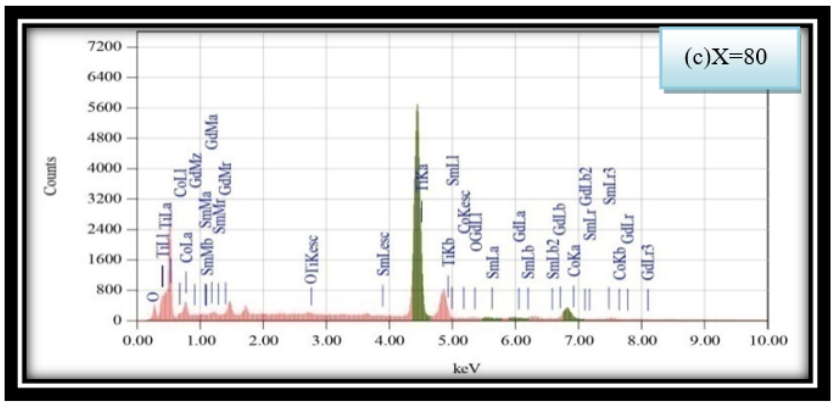

Element line	Weight %	Atom %
Ti L	82.15	85.64
Co L	15.85	12.06
Sm L	1.02	1.06
Gd L	1.01	1.24
Total	100.00	100.00

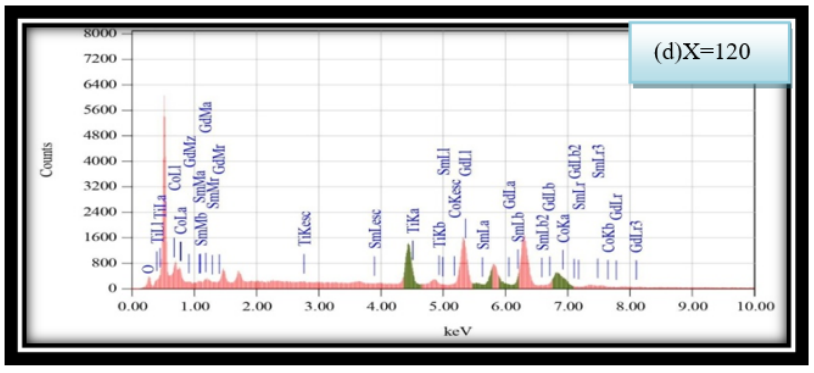

Element line	Weight %	Atom %
Ti L	83.05	85.45
Co L	14.69	12.18
Sm L	1.11	1.24
Gd L	1.15	1.12
Total	100.00	100.00

Fig. 7. Results of Energy Dispersive Spectroscopy EDS of (Ti-Co-RE) NEG material.

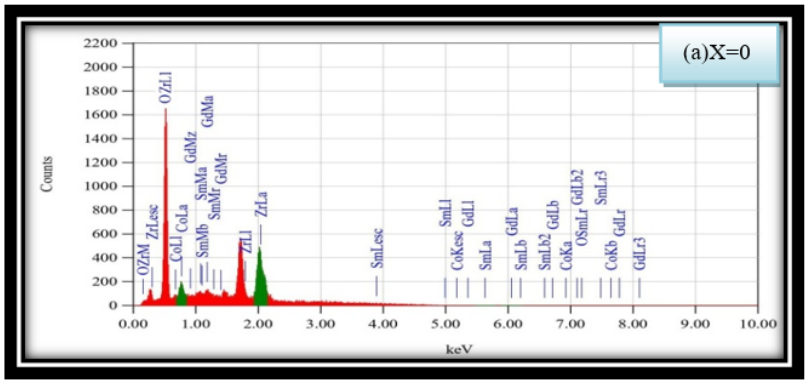

Element line	Weight %	Atom %
Zr L	81.14	73.66
Co L	16.64	24.02
Sm L	1.12	0.99
Gd L	1.09	1.32
Total	100.00	100.00

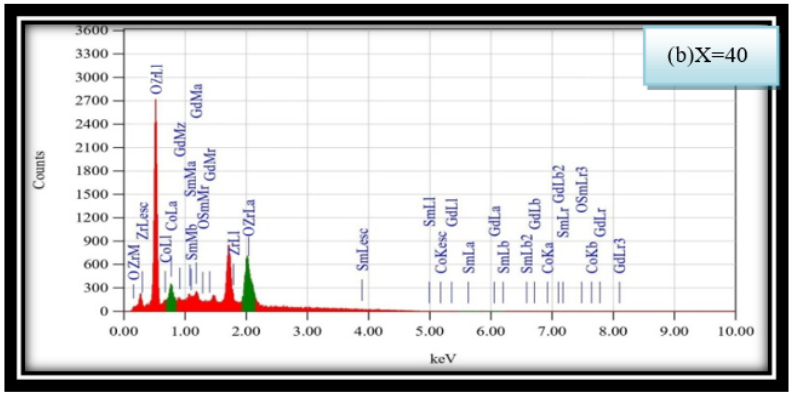

Element line	Weight %	Atom %
Zr L	74.40	65.47
Co L	23.55	32.68
Sm L	1.05	1.04
Gd L	0.93	0.81
Total	100.00	100.00

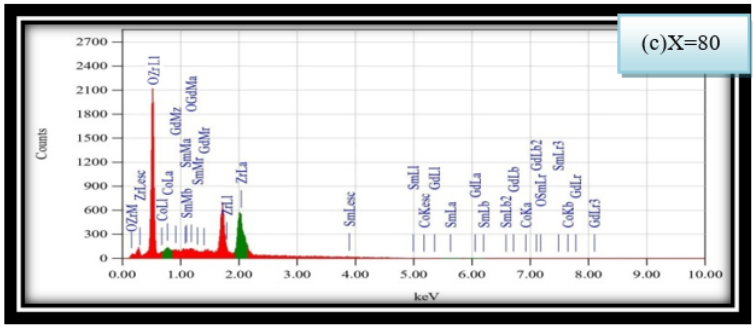

Element line	Weight %	Atom %
Zr L	91.84	88.89
Co L	5.92	9.25
Sm L	1.32	0.90
Gd L	0.92	0.96
Total	100.00	100.00

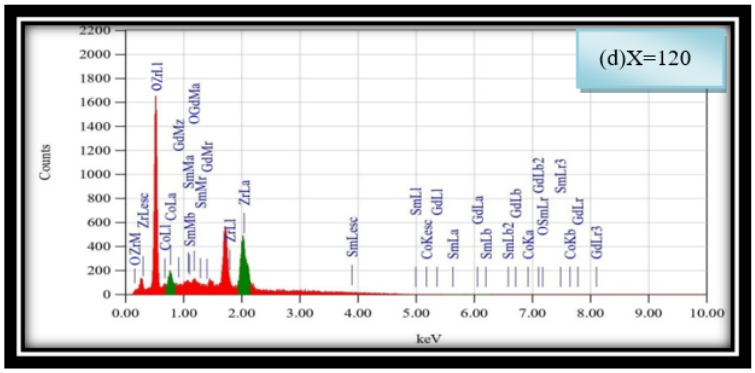

Element line	Weight %	Atom %
Zr L	91.59	88.50
Co L	6.20	9.65
Sm L	1.26	0.86
Gd L	0.95	0.99
Total	100.00	100.00

Fig. 8. Results of Energy Dispersive Spectroscopy EDS of (Ti-Co-RE) NEG material.

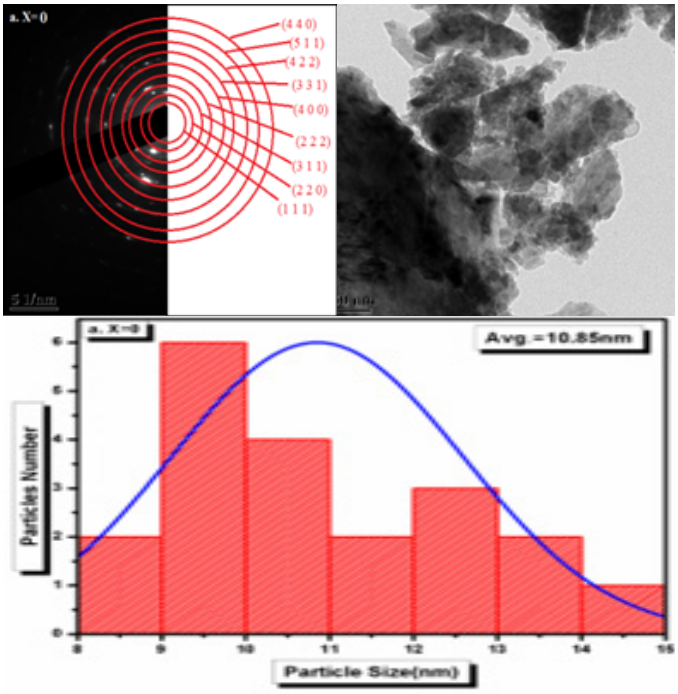

Fig. 9. TEM images and particle size distribution histogram of (Ti-Co-RE) lower concentration (X=0).

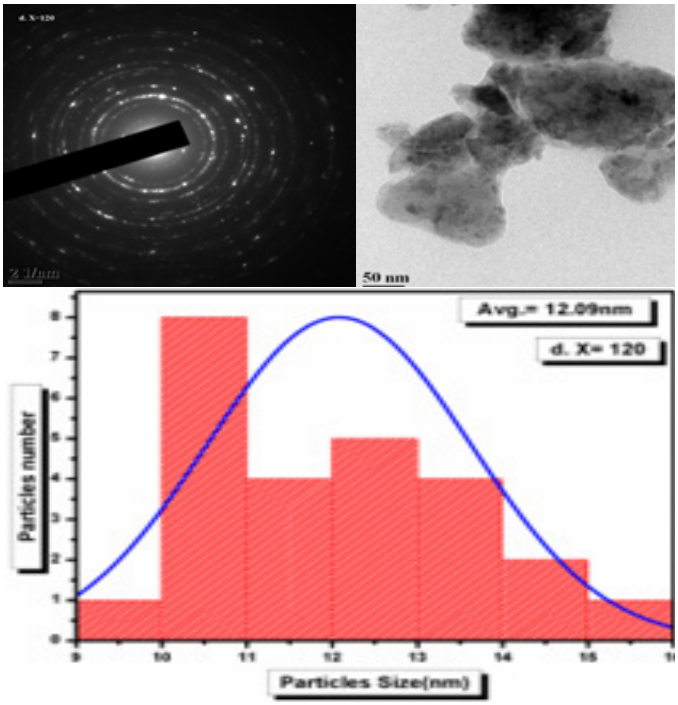

Fig. 10. TEM images and particle size distribution histogram of (Ti-Co-RE) higher concentration (X=120).

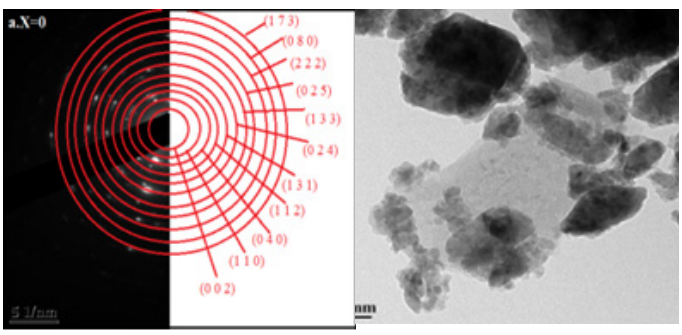

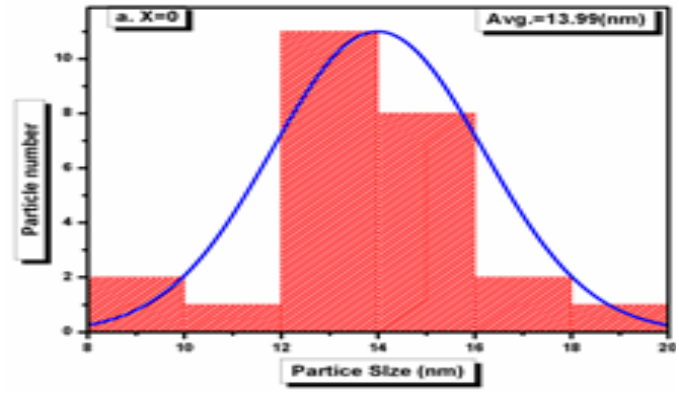

Fig. 11. TEM images and particle size distribution histogram of (Zr-Co-RE) lower concentration

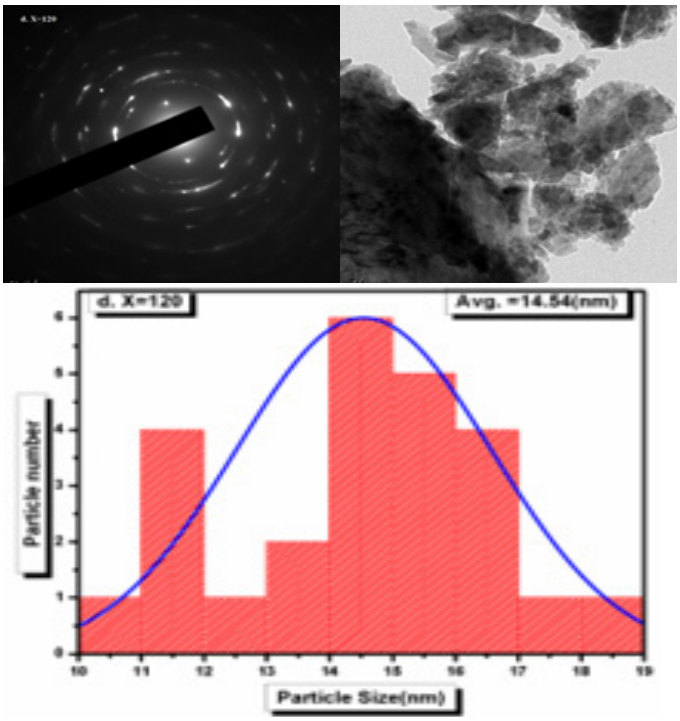

Fig. 12. TEM images and particle size distribution histogram of (Zr-Co-RE) higher concentration (X=120).

evaporable getter materials are shown in Fig.9 to 12. The grain distribution in these photos is uniform. Lower and higher concentrations have average particle sizes of 10.85nm (X=0) and 12.09nm (X=120), respectively [Straumal, Boris B., et al (2019)]. It was discovered that as the titanium concentration increased, the average particle size also increased. Lower and higher concentrations have average particle sizes of 10.85nm (X=0) and 12.09nm (X=120), respectively.

Furthermore, it was discovered that as the titanium concentration increases, the average particle size increases [Ellingham, et al (2017)]. The second NEG series (Zr-Co-RE) demonstrates the formation of an orthorhombic crystal structure of Zr_3Co.

Lower and higher concentrations have average particle sizes of 13.99nm (X=0) and 14.54nm (X=120), respectively. When RE concentrations are added, the average particle size and d-spacing increase. The TEM micrographs in the pictures show that the NEG materials effectively absorb residual gases in both cases. The fact that the two series, nano-sized Ti_2Co and Zr_3Co, may improve the specific surface area and grain boundaries, allowing for fast gas diffusion, is remarkable. Because of the microstructure alteration, this could be an excellent way to increase the sorption capacity of NEG materials [Bourim, El-Mostafa; (2018); Rokosz, Krzysztof, et al (2016)].

4. Conclusions

The effects of samarium and gadolinium (RE) in Ti-Co and Zr-Co non-evaporable getters are investigated in the present study, and the following conclusions are established.

a. The non-evaporable getter materials (Ti-Co-RE) and (Zr-Co-RE) were effectively synthesized at a temperature of 1000°C, and their sorption properties were investigated.

b. According to the XRD results in both series, when the cobalt content lowers, the FWHM reduces. Interatomic spacing, lattice constant(a), cell volume(V), crystalline size (D), and Intensity(I) are all growing, and phase changes were shown in both series. When the lattice parameter is increased in both series, the NEG absorb the remaining gases more efficiently. The surface of the getter begins to pump more gases into the getter when these parameters are increased.

c. TG and DTA experimental results in the (Ti-Co-RE) series demonstrate that nitrogen sorption increases from 450°C to 950°C and physisorbed gas desorption rises from 30°C to 450°C. In the (Zr-Co-RE) series, the temperature increases from 300°C to 310°C, resulting in the desorption of physisorbed gases from the getter. After that, the temperature increases from 310°C to 950°C. The getter gradually enhances nitrogen sorption. This is a positive sign if the materials are NEG.

d. The SEM with EDS study indicated that sintering at higher temperatures results in porous pellets with increased specific surface area and gas sorption capacity in both series. In addition, the EDS graphs revealed the getter material's optimal weight and atomic percentage.

e. According to TEM microstructure investigations, the crystalline size of XRD patterns is proportional to the rise in particle size in a series; the histogram patterns can illustrate given above. The adsorption capacities of the non-evaporable getter materials increase as the activation temperature increases.

References

[1.] Ashiri, R. (2013)"Detailed FT-IR spectroscopy characterization and thermal analysis of synthesis of barium titanate nanoscale particles through a newly developed process." Vibrational Spectroscopy 66: 24-29.

[2.] Ashiri, Rouholah. (2012)"Analysis and characterization of phase evolution of nano-sized batio 3 powder synthesized through a chemically modified sol-gel process." Metallurgical and Materials Transactions A 43, no. 11: 4414-4426.

[3.] Bamne, Jyoti, Kajol Taiwade, P. K. Sharma, and Fozia Z. Haque. (2018) "Effect of calcination temperature on the growth of TiO2 nanoparticle prepared via sol-gel method using triton X-100 as surfactant." In AIP Conference Proceedings, vol. 2039, no. 1, p. 020076. AIP Publishing LLC,.

[4.] Bandyopadhyay, Debashis, R. C. Sharma, and N. Chakraborti. (2000) "The Ti-Co-C system (titanium-cobalt-carbon)." Journal of phase equilibria 21, no. 2 :179-185.

[5.] Behnajady, Mohammad A., and Hamed Eskandarloo. (2015) "Preparation of TiO 2 nanoparticles by the sol–gel method under different pH conditions and modeling of photocatalytic activity by artificial neural network." Research on Chemical Intermediates 41, no. 4: 2001-2017.

[6.] Bourim, El-Mostafa; Kim, Hee; Chung, Nak-Kwan (2018). Development and Characterization of Non-Evaporable Getter Thin Films with Ru Seeding Layer for MEMS Applications. Micromachines, 9(10), 490.

[7.] Bu, J. G., C. H. Mao, Y. Zhang, X. Y. Wei, and J. Du. (2012) "Preparation and sorption characteristics of Zr–Co–RE getter films." Journal of alloys and compounds 529: 69-72.

[8.] Co O2 : Lambert, S. Leligny, H. Grebille, D.,

(2001) Journal of Solid State Chemistry4.

[9.] David R. Gaskell, (1995) Introduction to the Thermodynamics of Materials, Taylor & Francis, Washington, p. 356, 3rd.

[10.] Deng, Guangxia, Xushan Zhao, Shumao Wang, Xiaopeng Liu, Zhinian Li, and Lijun Jiang. (2013) "Characterization of Ti-based hydrogen absorbing alloys." International journal of hydrogen energy 38, no. 29: 13050-13054.

[11.] Ellingham, Sarah T. D.; Thompson, Tim J. U.; Islam, Meez (2017). Scanning Electron Microscopy-Energy-Dispersive X-Ray (SEM/EDX): A Rapid Diagnostic Tool to Aid the Identification of Burnt Bone and Contested Cremains. Journal of Forensic Sciences, (), –. doi:10.1111/1556-4029.13541.

[12.] Garcia, JoelsonCott, L. M. R. Scolfaro, A. T. Lino, V. N. Freire, G. A. Farias, C. C. Silva, HW Leite Alves, S. C. P. Rodrigues, and E. F. da Silva Jr. (2006) "Structural, electronic, and optical properties of Zr O 2 from ab initio calculations." Journal of Applied Physics 100, no. 10: 104103.

[13.] GoodarzNaseri, Mahmoud, Elias B. Saion, Hossein AbbastabarAhangar, Abdul Halim Shaari, and Mansor Hashim. (2010) "Simple synthesis and characterization of cobalt ferrite nanoparticles by a thermal treatment method." Journal of Nanomaterials.

[14.] Heshmatpour, Felora, and Reza BabadiAghakhanpour. (2011)"Synthesis and characterization of nano-crystalline zirconia powder by simple sol–gel method with glucose and fructose as organic additives." Powder Technology 205, no. 1-3: 193-200.

[15.] Heyder, R., L. Watson, R. Jackson, G. Krueger, and A. Conte. (1996) "Non-evaporable gettering technology for in-situ vacuum processes." Solid state technology 39, no. 8: 71-74.

[16.] J.T. Ellingham, J. Soc. Chem. Ind. 63 (1944) 125.

[17.] Keiteb, Aysar S., Elias Saion, Azmi Zakaria, and NayerehSoltani. (2016)"Structural and optical properties of zirconia nanoparticles by thermal treatment synthesis." Journal of nanomaterials .

[18.] Larson, Erica J., Katie J. Cook, Joseph R. Wermer, and Dale G. Tuggle. (2002) "Nitriding reactions with a Zr–Mn–Fe metal getter." Journal of alloys and compounds 330: 897-901.

[19.] Li, Chien-Cheng, Jow-Lay Huang, Ran-Jin Lin, and Ding-FwuLii. (2006) "Preparation and characterization of non-evaporable porous Ti–Zr–V getter films." Surface and Coatings Technology 201, no. 7: 3977-3981.

[20.] Moghadam, A. Heidary, V. Dashtizad, A. Kaflou, and H. Yoozbashizadeh. (2015) "Effect of rare earth elements on sorption characteristics of nanostructured Zr–Co sintered porous getters." Vacuum 111: 9-14.

[21.] Moghadama, A. Heidary, V. Dashtizad, A. Kaflou, and H. Yoozbashizadeh. (2015)"Effect of RE Elements on the Sorption Properties of Nanocrystalline Zr-Co Getters Prepared by Mechanical Alloying." In Proceedings of the TMS Middle East—Mediterranean Materials Congress on Energy and Infrastructure Systems (MEMA 2015), pp. 273-282. Springer, Cham,.

[22.] N. Bekris et al., (2000) "On the Thermal Stability of the Zirconium/Cobalt-Hydrogen System", Fusion Eng. Des. 49-50, 781-789.

[23.] Naseri, Mahmoud Goodarz, Elias B. Saion, Hossein AbbastabarAhangar, Mansor Hashim, and Abdul Halim Shaari. (2011) "Simple preparation and characterization of nickel ferrite nanocrystals by a thermal treatment method." Powder Technology 212, no. 1: 80-88.

[24.] Petti, Daniela, Matteo Cantoni, Marco Leone, Riccardo Bertacco, and E. Rizzi. (2010) "Activation of Zr–Co–rare earth getter films: An XPS study." Applied Surface Science 256, no. 21: 6291-6296.

[25.] Phromma, Siripond, TuksadonWutikhun, PanitaKasamechonchung, TippabustEksangsri, and Chaweewan Sapcharoenkun. (2020) "Effect of calcination temperature on photocatalytic activity of synthesized TiO2 nanoparticles via wet ball milling sol-gel method." Applied Sciences 10, no. 3: 993.

[26.] Qian, Z., and J. L. Shi. (1998) "Characterization of pure and doped zirconia nanoparticles with infrared transmission spectroscopy." Nanostructured materials 10, no. 2: 235-244.

[27.] Rokosz, Krzysztof, Tadeusz Hryniewicz, Dalibor Matýsek, Steinar Raaen, Jan Valíček, Łukasz Dudek, and Marta Harničárová. (2016) "SEM, EDS and XPS analysis of the coatings obtained on titanium after plasma electrolytic oxidation in electrolytes containing copper

nitrate." Materials 9, no. 5: 318.

[28.] Rostoker, W., (1952) "Transactions of the American Institute of Mining, Metallurgical and Petroleum En, 194.

[29.] S. Konish et al, (1995) "Reversible Disproportionation of ZrCo under High Temperatrue and Hydrogen Pressure", J. Nuclear Materials, 223, 294-299.

[30.] Sato, Shintaro, Akio Kawabata, Daiyu Kondo, Mizuhisa Nihei, and Yuji Awano. (2005) "Carbon nanotube growth from titanium–cobalt bimetallic particles as a catalyst." Chemical Physics Letters 402, no. 1-3: 149-154.

[31.] Song, Ho-Jun, Mi-Kyung Han, Hyeon-GyeongJeong, Yong-Tai Lee, and Yeong-Joon Park. (2014) "Microstructure analysis of Ti-xPt alloys and the effect of Pt content on the mechanical properties and corrosion behavior of Ti alloys." Materials 7, no. 5: 3990-4000.

[32.] Straumal, B. B., A. R. Kilmametov, Yu Ivanisenko, A. A. Mazilkin, R. Z. Valiev, N. S. Afonikova, A. S. Gornakova, and H. Hahn. (2018) "Diffusive and displacive phase transitions in Ti–Fe and Ti–Co alloys under high pressure torsion." Journal of Alloys and Compounds 735: 2281-2286.

[33.] Straumal, Boris B., Anna Korneva, Askar R. Kilmametov, Lidia Lityńska-Dobrzyńska, Alena S. Gornakova, Robert Chulist, Mikhail I. Karpov, and PawełZięba. (2019) "Structural and mechanical properties of Ti–Co alloys treated by high pressure torsion." materials 12, no. 3: 426.

[34.] Surendra, K., and A. D. P. Rao. (2022) "Synthesis, characterization, and thermal analysis of Ti-Co, Zr-Co, Ti-Co-RE and Zr-Co-RE based non-evaporable getter materials." *Materials Today: Proceedings* 60: 144-152.

[35.] Valdre, G., D. Zacchini, R. Berti, A. Costa, A. Alessandrini, P. Zucchetti, and U. Valdre. (1999) "Nitrogen sorption tests, SEM-windowless EDS and XRD analysis of mechanically alloyed nano-crystalline getter materials." Nanostructured Materials 11, no. 6: 821-829.

[36.] Wesley W.M. Wendlandt, (1986) Thermal Analysis, 3rd ed. (John Wiley & Sons, Inc., New York, USA, pp.137, 181.

[37.] Wu, Jun. (2012) "In-situ, real-time TEM observation of pressure-induced anatase to alpha-PbO2-type phase transition in nano-crystalline TiO2." Microscopy and Microanalysis 18, no. S2: 1710-1711

[38.] Xiong, Y. H., X. Y. Wei, G. R. Qin, P. Yuan, C. H. Mao, and J. Du. (2008) "Preparation and hydrogen sorption performance of a modified Zr–C getter." Vacuum 82, no. 8: 737-741.

[39.] Xu, Yao Hua, Yao Zong Sui, Xiao Zhang, Hao Liu, Peng Yuan, and Feng Wei. (2019) "Activation Process and Mechanism of ZrCoCe Getter Films." In Materials Science Forum, vol. 944, pp. 613-618. Trans Tech Publications Ltd,.

[40.] Xu, Yaohua, Jiandong Cui, Hang Cui, Hao Zhou, Zhimin Yang, and Jun Du. (2016) "Influence of deposition pressure, substrate temperature and substrate outgassing on sorption properties of Zr–Co–Ce getter films." Journal of Alloys and Compounds 661: 396-401.

[41.] Xu, Yaohua, Jiandong Cui, Hang Cui, Hao Zhou, Zhimin Yang, and Jun Du. (2016) "ZrCoCe getter films for MEMS vacuum packaging." Journal of Electronic Materials 45, no. 1: 386-390.

[42.] Yoozbashizadeh, Hossein, Ali Heidary Moghadam, ValiollahDashtizad, and Ali Kaflou. (2015) "Effect of Rare Earth Elements on the Sorption Characteristics of Nanostructured Zr-base Sinter Porous Getter Prepared by Mechanical Alloying." International Journal of Research in Materials Science 1, no. 1: 3-12.

[43.] Yu, T.-H. Lin, S.-J. Chao, P. Fang, C.-S. Huang, C.-S., (1974) Acta GeologicaSinica, **2**.

[44.] Yuan, Peng, Yao Zong Sui, Xiao Zhang, Hao Liu, Feng Wei, and Yao Hua Xu. (2019) "Preparation and Characterization of Ni/ZrCoCe Stack Getter Films." In Materials Science Forum, vol. 944, pp. 619-624. Trans Tech Publications Ltd.

[45.] Yun, S. H., S. Cho, M. H. Chang, H. G. Kang, K. J. Jung, H. Chung, D. Koo, K. M. Song, K. I. Kim, and T. W. Hong. (2010)" Variation of PCT Isotherm in the Disproportionated ZrCo. No. IAEA-CN—180".

[46.] Zavaliy, I. Yu, R. V. Denys, R. Černý, I. V. Koval'chuck, G. Wiesinger, and G. Hilscher. (2005) "Hydrogen-induced changes in crystal structure and magnetic properties of the Zr3MOx (M= Fe, Co) phases." Journal of alloys and compounds 386, no. 1-2: 26-34.

[47.] Zhang, Y., X. Y. Wei, C. H. Mao, T. F. Li, P. Yuan, and J. Du. (2009) "Preparation and pumping characteristics of Ti–7.5 wt.% Mo getter." Journal of alloys and compounds 485, no. 1-2: 200-203.

[48.] Zhao, Zhenmei, Xiuying Wei, YuhuaXiong, and Changhui Mao. (2009) "Preparation of Ti-Mo getters by injection molding." Rare Metals 28, no. 2: 147-150.

[49.] Zhou, Chao, Detian Li, Hui Zhou, Xingguang Liu, and Zhanji Ma. (2020) "Influence of the sputtering glancing angle on the microstructure and adsorption characteristics of (Zr-Co-RE) getter films." Materials Research Express 7, no. 3: 036402.

[50.] ZHOU, Hong-guo, Xiu-ying WEI, Chang-hui MAO, Yu-hua XIONG, and Guang-rong QIN. (2007) "Effects of Mo on the microstructure and hydrogen sorption properties of Ti-Mo getters." Chinese Journal of aeronautics 20, no. 2: 172-176.

[51.] Zr O2: (1987) Suyama, R. Horiuchi, H. Kume, S., Yogyo-Kyokai-Shi, 95.

[52.] Zr3Co: (1970) Kripyakevich, P.I. Burnashova, V.V. Markiv, V.Ya., Dopovidi Akademii Nauk Ukrainskoi RSR, Seriya A: Fiziko-Tekhnichni ta Matematich, 1970.